Thermoelectric properties of orthorhombic silicon allotrope Si (oP32) from first-principles calculations*

Pei Zhang(张培), Tao Ouyang(欧阳滔)†, Chao Tang(唐超), Chao-Yu He(何朝宇), Jin Li(李金), Chun-Xiao Zhang(张春小), and Jian-Xin Zhong(钟建新)‡

Hunan Key Laboratory for Micro-Nano Energy Materials & Device and School of Physics and Optoelectronics, Xiangtan University, Xiangtan 411105, *China*

(Received 5 May 2020; revised manuscript received 29 June 2020; accepted manuscript online 6 July 2020)

The diamond-like cubic silicon (d-Si) is widely used in modern electronics and solar cell industries. However, it is not an optimal candidate for thermoelectric application due to its high lattice thermal conductivity. Si (oP32) is a recently predicted orthorhombic silicon allotrope, whose total energy is close to that of d-Si. Using first-principles calculations and Boltzmann transport theory, we systematically investigate the thermoelectric properties of Si (oP32). The lower phonon thermal conductivity and higher power factor are obtained in Si (oP32) than those in diamond silicon. The low phonon thermal conductivity (33.77 W/mK at 300 K) is mainly due to the reduction of the phonon group velocity and enhancement of phonon–phonon scattering (including scattering phase space and strength). Meanwhile, the results also show that the thermoelectric performance along the *zz* lattice direction is better than that along the *xx* and *yy* lattice directions, and the figure of merit (700 K) along the *zz* lattice direction could approach to 2.45 and 1.75 for p-type and n-type Si (oP32), respectively. The values are much higher than those of d-Si (about 0.06)) and Si_{24} (0.6), indicating that the Si (oP32) is a promising candidate for thermoelectric applications. Our theoretical studies shed light on the thermoelectric properties of Si (oP32) and could stimulate further experimental studies.

Keywords: thermoelectric, Si (oP32), lattice thermal conductivity, first-principles

PACS: 84.60.Rb, 74.25.fc, 74.25.Kc, 63.20.dk **DOI:** 10.1088/1674-1056/aba2e1

1. Introduction

With the depletion of fossil fuel, the search for renewable energy sources and related energy materials is becoming more and more urgent. Thermoelectric (TE) materials,[1–3] which can direly convert waste heat into electricity, have attracted much attention in the past few decades. However, low conversion efficiency and high production costs have greatly hindered them from being put into commercial applications for decades.[4] Usually, the efficiency of thermoelectric device is determined by the dimensionless figure of merit, defined as $ZT = S^2\sigma T/(\kappa_e + \kappa_l)$,[5,6] where S, σ, T, κ_e, and κ_l are the Seebeck coefficient, electrical conductivity, absolute temperature, electronic thermal conductivity, and lattice (phonon) thermal conductivity, respectively. Obviously, in order to achieve high thermoelectric performance, high power factor ($S^2\sigma$) and (or) low thermal conductivity are (is) needed. Nevertheless, this is not easy to optimize one of these parameters without affecting other ones due to complex competition among electronic transport coefficients.[7] Therefore, seeking potential materials with low thermal conductivity and improving thermoelectric properties of materials has become a hot topic in the present thermoelectricity research field.[8–11]

Silicon is one of the most abundant elements in Earth's crust, next to oxygen. Of the silicon crystal structures, diamond silicon (d-Si) is the most stable phase thermodynamically under normal temperature and pressure conditions. Due to its appropriate combination of structural, chemical, mechanical, and electronic properties, it is the most widely used silicon single crystal structure in modern electronics and solar cell industries.[12] Such an Si-based material (d-Si), however, has high lattice thermal conductivity (140 W/mK),[13] so, it is not an optimal candidate for thermoelectric applications (the ZT is merely 0.01 at room temperature).[14–16] Therefore, exploration of new silicon allotropes has attracted considerable attention in recent decades due to the wide applications of silicon materials. As a result, many new thermodynamically stable silicon structures have been predicted,[17–22] such as Si_{24},[18] M585-Si,[21] and tP36-Si.[22] It is worth mentioning that Si_{24} (orthorhombic *Cmcm*) has been successfully produced through a novel high-pressure precursor process.[18]

Very recently, Oreshonkov *et al.* reported a new orthorhombic Si allotrope Si (oP32) with a structure belonging to space group *Pbcm*.[23] Their results show that the total energy per formula unit for the Si (oP32) structure is lower than the one for *Cmcm* silicon (Si_{24}). Besides, germanium allotrope Ge (oP32) with the same space group has been synthesized by

*Project supported by the Program for Changjiang Scholars and Innovative Research Team in University, China (Grant No. IRT13093), the National Natural Science Foundation of China (Grant Nos. 11304262 and 11404275), the Scientific Research Fund of Hunan Provincial Education Department, China (Grant Nos. 17B252, 17K086, and 16K084), the Natural Science Foundation of Hunan Province, China (Grant No. 2016JJ3118), and the Xiangtan University Innovation Foundation for Postgraduate, Hunan Province, China (Grant No. XDCX2020B095).

†Corresponding author. E-mail: ouyangtao@xtu.edu.cn

‡Corresponding author. E-mail: jxzhong@xtu.edu.cn

© 2020 Chinese Physical Society and IOP Publishing Ltd

the mild-oxidation/ delithiation of Li_7Ge_{12} in ionic liquids.[24] Thus, it can be reasonably assumed that Si (oP32) will be prepared in future experiments. Up to now, thermoelectric transport property of Si (oP32) has not been reported in theory and experiment. In this work, we provide a comprehensive study of the electronic and phonon transport properties of Si (oP32) based on first-principles calculations and Boltzmann transport theory. The results indicate that compared with d-Si, the Si (oP32) presents a very low lattice thermal conductivity and moderate power factor. Further analyses of phonon velocity and Grüneisen parameters are provided to explain its low lattice thermal conductivity. The maximum ZT value of 2.42 (1.74) can be achieved by the optimal p-type (n-type) doping at 700 K along the zz crystal direction. This value is substantially larger than that of d-Si and Si_{24}, indicating that Si (oP32) is a promising thermoelectric material. The rest of the paper is organized as follows. In Section 2, we give a brief description of the calculation method of first-principles and transport coefficients. In Section 3, we show the results on the thermoelectric transports in Si (oP32), including the detailed description of electronic and phonon transports. Finally, some conclusions are drawn from the present study in Section 4.

2. Computational details

In the present work, all first-principles calculations are carried out based on density functional theory (DFT) through using the projector augmented wave (PAW) pseudopotential, as implemented in the Vienna *ab initio* simulation package (VASP).[25–27] The generalized gradient approximation (GGA) with Perdew–Burke–Ernzerhof (PBE) exchange–correlation functional is used.[28] A plane-wave basis set with an energy cutoff of 400 eV and a $4 \times 3 \times 4$ k-mesh is adopted to sample the reciprocal space of the primitive unit cell of Si (oP32). The geometric structure is fully optimized until the residual forces on atoms are smaller than 0.001 eV/Å. Moreover, the energy convergence threshold is set to be 10^{-6} eV for the self-consistent field (SCF) procedure. As the band gap is underestimated when the PBE functional is adopted to calculate the electronic structure, the modified Becke–Johnson (mBJ) exchange potential is introduced to acquire a more accurate energy band structure.[29–31]

Using the ShengBTE code with the harmonic second-order interatomic force constants (2nd IFCs) and anharmonic third-order IFCs (3rd IFCs) as input files,[32] the phonon transport properties are obtained by iteratively solving the phonon Boltzmann transport equation (PBTE). The phonon dispersion and the 2nd IFCs are calculated by using VASP and PHONONPY packages with $2 \times 1 \times 2$ supercell and $3 \times 3 \times 3$ k-mesh.[33] The anharmonic 3rd IFCs are calculated by utilizing the same supercell and k-mesh with an interaction range being cut off up to the sixth nearest neighbor. A phonon q-grid of $7 \times 5 \times 7$ is used to calculate the lattice thermal conductivity of Si (oP32). The electronic transport properties can be acquired by using the semi-classical Boltzmann transport theory and the rigid band approach as implemented in BoltzTrap.[34] The electronic relaxation time is treated in the framework of deformation potential (DP) theory.[35] In order to obtain the reliable electronic transport coefficients, a denser k-mesh in the first Brillouin zone (BZ) is chosen.

3. Results and discussion

3.1. Atomic and electronic structure

The primitive cell of silicon allotropes Si (oP32) is shown in Fig. 1(a). As illustrated in Fig. 1(a), the Si (oP32) has an orthorhombic structure belonging to space group *Pbcm* (No. 57). The calculated lattice constants of Si (oP32) are $a = 7.91$ Å, $b = 11.38$ Å, and $c = 7.49$ Å, which are in good agreement with earlier theoretical prediction.[23] Here, a, b, and c axes correspond to x, y, and z directions, respectively. As is well known, the electronic structure of a material plays an important role in its transport properties. The calculated energy band structure and corresponding electronic density of states (DOS) of Si (oP32) are presented in Figs. 1(b) and 1(c).

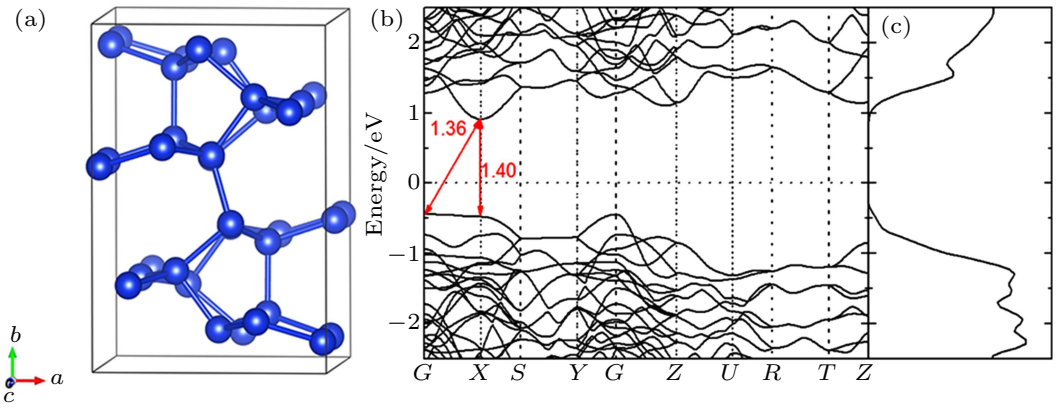


Fig. 1. (a) Crystal structure of Si (oP32), (b) electronic band structure, and (c) electronic density of states (DOS) of Si (oP32). The special point coordinates in Brillouin zone are G (0, 0, 0), X (0.5, 0, 0), S (0.5, 0.5, 0), Y (0, 0.5, 0), G (0, 0, 0), Z (0, 0, 0.5), U (0.5, 0, 0.5), R (0.5, 0.5, 0.5), T (0, 0.5, 0.5), and Z (0, 0, 0.5).

Obviously, Si (oP32) is a semiconductor with the valence band maximum (VBM) and conduction band minimum (CBM) located at X and G points, respectively. The direct and indirect band gap are calculated to be 1.40 eV and 1.36 eV, respectively, which are consistent with the values obtained in earlier work.[23] Besides, the trend of the band structure also presents similar behaviors to those in previous work, indicating the reliability of our approach.[23]

3.2. Phonon transport properties

We first verify the phonon dispersion curves of Si (oP32), which are obtained by solving the eigenvalues of the harmonic 2nd IFCs matrix. As shown in Fig. 2(a), there are no phonon branches with imaginary frequencies in the whole BZ, indicating that the Si (oP32) is dynamically stable at ambient pressure. There exist three acoustic and ninety-three optical phonon branches corresponding to the thirty-two atoms' primitive cell of Si (oP32). The maximum frequency of the optical phonon modes of Si (oP32) is about 15.25 THz, which is a little higher than that of d-Si (15.06 THz).[36] We also find that the lowest optical modes overlap with its acoustic branches, resulting in a strong coupling of acoustic and optical modes and lower lattice thermal conductivity. Moreover, it is found that most of the phonon branches are very flat, making phonons easily satisfy the conservation of energy and momentum. And it will be discussed later.

Lattice thermal conductivity is an extremely important physical quantity to evaluate the ability of material to implement the thermal transport. Based on the self-consistent iterative method,[37–39] κ_l can be obtained from the following formula:

$$\kappa_l = \frac{1}{V}\sum_i C_{i,\boldsymbol{q}} v_{i,\boldsymbol{q}}^2 \tau_{i,\boldsymbol{q}}, \tag{1}$$

where V is the primitive cell volume, $C_{i,\boldsymbol{q}}$, $v_{i,\boldsymbol{q}}$, and $\tau_{i,\boldsymbol{q}}$ are the mode specific heat capacity, phonon group velocity, and relaxation time, respectively, for the phonon mode i at the wavevector $\boldsymbol{q}$. The average lattice thermal conductivity of Si (oP32) as a function of temperature is presented in Fig. 3(a), which is calculated from $\kappa_l = (\kappa_{xx} + \kappa_{yy} + \kappa_{zz})/3$. For comparison, the lattice thermal conductivity of d-Si is also plotted in Fig. 3(a). It can be seen that the lattice thermal conductivity of Si (oP32) and d-Si decrease with temperature increasing. This phenomenon is caused by the enhanced phonon–phonon scattering at higher temperature. In all temperature ranges that we are studying, the lattice thermal conductivity of Si (oP32) is significantly lower than that of d-Si. The thermal conductivity of Si (oP32) at 300 K along the three lattice directions and the average thermal conductivity of Si (oP32) and d-Si at this temperature are shown in Fig. 3(b). The anisotropic factor ($|\kappa_\alpha - \kappa_{\text{ave}}|/\kappa_{\text{ave}}$, $\alpha = xx, yy, zz$) is also plotted in the inset. One can find that the lattice thermal conductivity of Si (oP32) displays weak anisotropy. At room temperature (300 K), the minimum lattice thermal conductivity is 30.94 W/mK along the xx lattice direction, while the maximum lattice thermal conductivity is 37.38 W/mK along the zz lattice direction. It can also be seen that the average lattice thermal conductivity of Si (oP32) is 33.77 W/mK, which is only about a quarter of d-Si (137.45 W/mK).

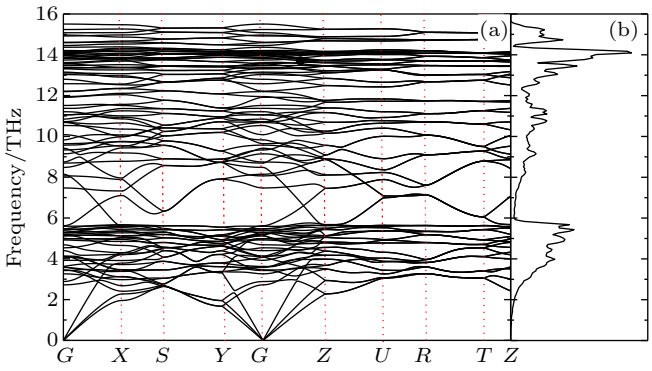


Fig. 2. (a) Phonon dispersion along different high-symmetry paths and (b) phonon density of states (PDOS) of Si (oP32).

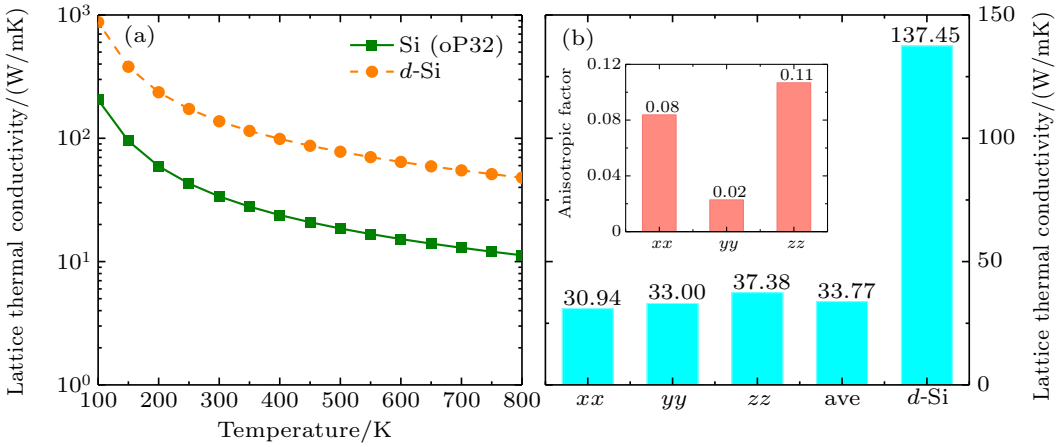


Fig. 3. (a) Calculated lattice thermal conductivity with respect to temperature for Si (oP32) and d-Si. (b) Lattice thermal conductivity of Si (oP32) and d-Si at 300 K and inset shows the anisotropic factor ($|\kappa_\alpha - \kappa_{\text{ave}}|/\kappa_{\text{ave}}$, $\alpha = xx, yy, zz$).

To have a further understanding of the low lattice thermal conductivity, we decompose the phonon mode properties of Si (oP32). From Fig. 4(a), large group velocities can be observed at low frequencies and relatively small at high frequencies. Meanwhile, it is clear that the phonon group velocity of Si (oP32) is smaller than that of d-Si. In addition to phonon group velocity, phonon relaxation time is another vital parameter to determine lattice thermal conductivity. Obviously, the phonon relaxation time of Si (oP32) is also smaller than that of d-Si. As is well known, the phonon relaxation time is governed by two main factors: the scattering strength and the phase space (scattering probability), which respectively quantify the intensity and number of phonon modes that can be scattered. The phonon scattering strength is quantified as the Grüneisen parameter (γ), which is plotted in Fig. 4(c). It can be found that the mode-level Grüneisen parameter (absolute value) of Si (oP32) is greater than that of d-Si, indicating that the phonon anharmonicity in Si (oP32) is much stronger than in d-Si. This phenomenon can be explained below. As plotted in Fig. 1(a), atoms in Si (oP32) are connected in the form of a triangular pyramid. However, compared with the ideal triangular pyramid of d-Si, the bond length and bond angle of Si (oP32) are deformed. For example, the bond lengths (angles) in Si (oP32) are in a range from 2.40 Å to 2.56 Å (93.7° to 126.8°). In such a case, phonons will encounter a stronger anharmonic scattering. The three-phonon scattering phase space (P3) of Si (oP32) and d-Si is shown in Fig. 4(d). As mentioned above, the acoustic phonon modes and optical phonon modes of Si (oP32) are mixed together, which makes it easier realize the requirements for energy conservation and quasi-momentum conservation of phonon scattering and thus leading to a lager P3 in Si (oP32). Therefore, one can conclude that the low lattice thermal conductivity of Si (oP32) is the consequence of the combined effect of the reduction of phonon group velocity and enhancement of phonon–phonon scattering (including scattering phase space and strength).

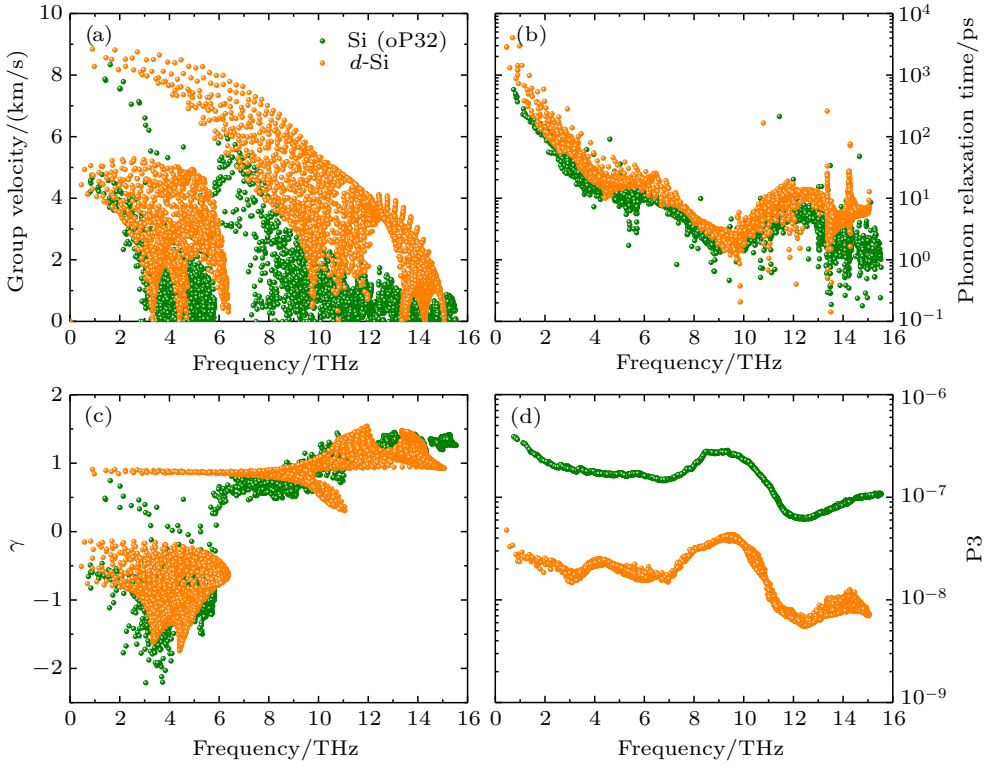


Fig. 4. (a) Group velocity, (b)phonon relaxation time, (c) Grüneisen parameter , and (d) three-phonon scattering phase space of Si (oP32) and d-Si *versus* frequency at room temperature.

3.3. Electrical transport properties

Using the semi-classical Boltzmann transport theory based on the rigid band approach, the electrical transport properties of Si (oP32) can be obtained. Since the output electrical transport coefficient is closely dependent on carrier relaxation time τ, a method to evaluate τ should be appropriately applied. Here, the deformation potential (DP) theory is adopted, which is a common method in previous researches.[40–44] Based on effective mass approximations, the carrier mobility μ and τ for three-dimensional (3D) semiconductor can be written as follows:[43]

$$\mu_{3D} = \frac{2\sqrt{2\pi}e\hbar^4 C_{3D}}{3\,(k_B T)^{3/2} m^{*5/2} E_l^2}, \tag{2}$$

$$\tau = \frac{\mu m^*}{e}, \tag{3}$$

where C_{3D} is the 3D elastic constant, E_l is the DP constant, and m^* is the effective mass along the transport direction. These

three quantities are easily derived from first-principles calculations. The other parameters e, $\hbar$, k_B, and T are the unit charge, reduced Planck constant, Boltzmann constant, and absolute temperature, respectively. The obtained parameters of Si (oP32) are all summarized in Table 1. Due to the anisotropic crystal structure, Si (oP32) shows an anisotropic transport character. The calculated carrier relaxation time of Si (oP32) along the zz lattice direction is larger than those along other lattice directions, which suggest that this lattice direction may exhibit a favorable thermoelectric property.

Table 1. Values of DP constant E_1, elastic constant C_{3D}, effective mass m^*, carrier mobility μ, and scattering time τ for electrons and holes along three directions in Si (oP32) at 300 K.

Carrier type	E_1/eV	C_{3D}/(eV/A^3)	m^*/m_e	μ/cm^2·V^{-1}·s^{-1}	$\tau/10^{-13}$ s
Electron (xx)	–8.54	0.876	0.836	327.06	1.56
Hole (xx)	–5.65		2.685	40.41	0.617
Electron (yy)	–10.30	0.930	0.221	6643.20	8.35
Hole (yy)	–8.69		0.660	605.53	2.23
Electron (zz)	–6.23	1.066	0.437	3785.53	9.40
Hole (zz)	–17.21		0.139	8693.76	6.87

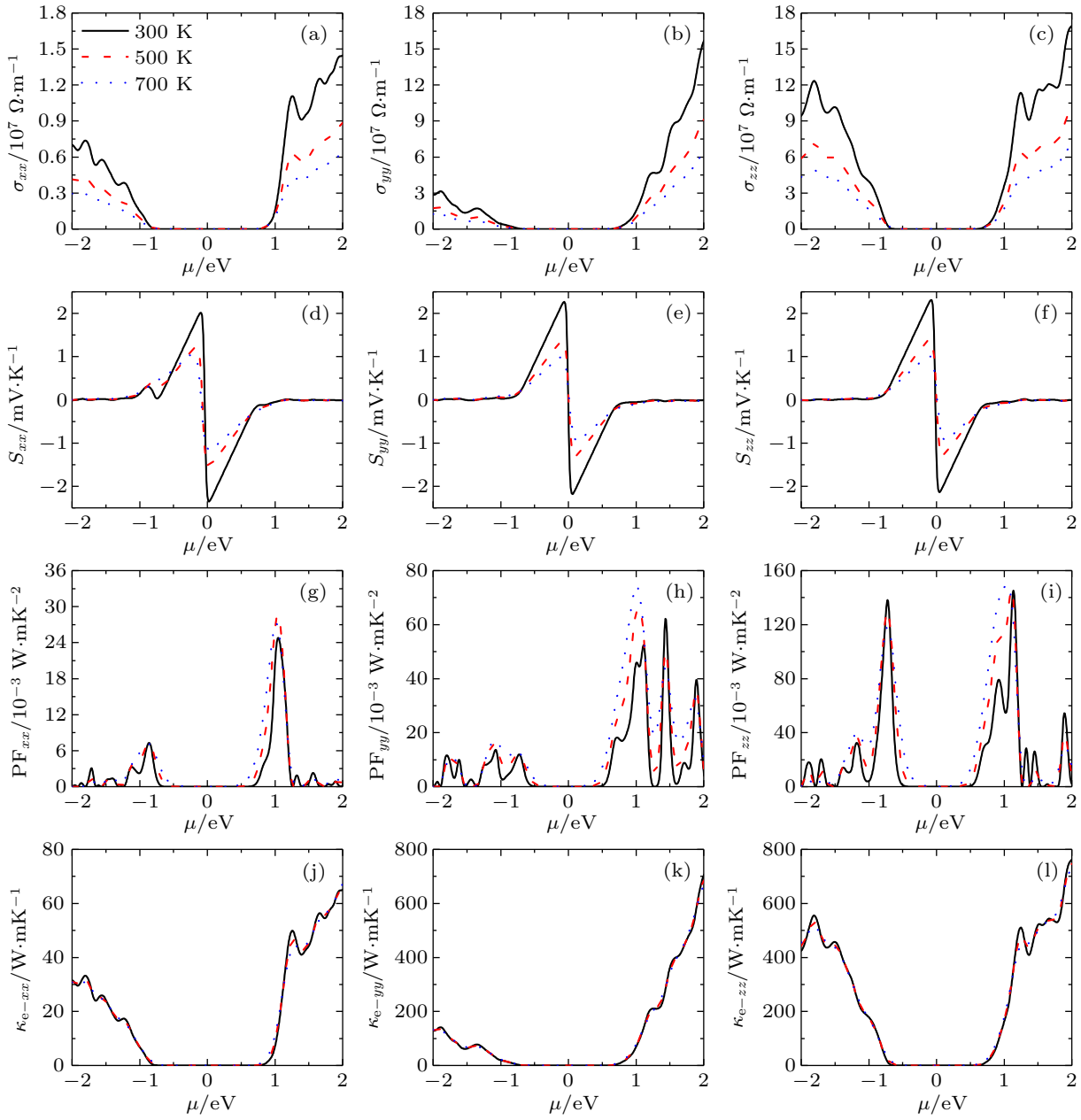


Fig. 5. Plots of [(a)–(c)] electrical conductivity, [(e)–(f)] Seebeck coefficient, [(g)–(i))] power factor, and [(j)–(l))] electronic thermal conductivity *versus* chemical potential at different temperatures along xx (left panels), yy (middle panels) and zz (right panels) directions.

The plots of electrical conductivity σ as a function of chemical potential under different temperatures are shown in Figs. 5(a)–5(c). Here, the positive and negative chemical potential correspond to n-type and p-type doping, respectively. One can see that σ decrease with temperature increasing, and, because the electrons obey the Fermi–Dirac distribution, the slope of σ around the VBM and CBM are flatted by increasing temperature. In addition, σ values of p-type material along the *xx* direction and the *yy* direction are smaller than those of n-type material, while, in the *zz* direction, the σ value of p-type is a little larger than that of n-type in the range of -1 eV$< \mu <$ 1 eV. Meanwhile, it can be noticed that σ displays an obviously anisotropic behavior where the σ value along the *zz* crystal direction is an order of magnitude larger than that along the *xx* directions. This difference can be understood from the values of carrier mobility μ and effective mass m^* along different directions.

We further present the calculated Seebeck coefficients *S* in Figs. 5(d)–5(f). It is obvious that the Seebeck coefficient slows down with temperature increasing. This phenomenon is a typical behavior of thermoelectric material and depends on its band gap. It should be noted that Si (oP32) exhibits relatively large Seebeck coefficient with weak anisotropy. For the *yy* and *zz* lattice direction, the Seebeck coefficients (absolute value) of the p-type Si (oP32) are slightly higher than those of n-type Si (oP32). However, the situation along the *xx* direction is opposite. At room temperature, the maximum Seebeck coefficient in p-type (n-type) can reach to 2.01 (2.35) mV/K, 2.27 (2.18) mV/K, and 2.32 (2.14) mV/K along the *xx*, *yy*, and *zz* directions, respectively, which are about four times larger than those of d-Si ($\sim$ 0.64 mV/K).[45]

Admirable thermoelectric material needs to have large Seebeck coefficient and electrical conductivity simultaneously. Power factor PF ($S^2\sigma$) is a good indicator to describe this joint effect of *S* and σ. We calculate the PF values and show them in Figs. 5(g)–5(i). It can be found that the power factors have a small difference at different temperatures. Moreover, it can be seen that for p- and n-type Si (oP32), the peaks of PF curves along the *zz* lattice direction are higher than those along the *xx* and *yy* lattice directions. Meanwhile, for all directions, the peaks of PF of n-type doping are always higher than those of p-type doping. At 300 K, the maximum PFs for n-type doping are 24.75 $\times$ 10^{-3}, 62.22 $\times$ 10^{-3}, and 145.10 $\times$ 10^{-3} W/mK^2 along the *xx*, *yy*, and *zz* lattice directions, respectively. Such large PFs of Si (oP32) are beneficial to the thermoelectric applications. The value of κ_e is calculated from the Wiedemann–Franz law $\kappa_e = L\sigma T$,[46] where $L = 1.5 \times 10^{-8}$ W$\cdot\Omega\cdot$K^{-2} is the Lorenz number.[47] As shown in Figs. 5(j)–5(l), the κ_e value of Si (oP32) possesses analogous curve to electrical conductivity and κ_e increases as the absolute value of the chemical potential increases.

3.4. Thermoelectric figures of merit

By combining the phonon and electron transport coefficient, we estimate the *ZT* values of Si (oP32) at three typical temperatures and plot them in Figs. 6(a)–6(c). One can note that the *ZT* value has an enhancing behavior with the increasing of temperature. Meanwhile, it can be seen that the two peaks of *ZT* value shift gradually towards the Fermi energy level ($\mu = 0$ eV), which is caused by reducing the band gap. The *ZT* value of p-type Si (oP32) is always lower than that of n-type Si (oP32) for each of *xx* and *yy* lattice directions, while the *ZT* value of Si (oP32) in p-type doping is lager that that in n-type doping for the *zz* direction. This phenomenon mainly stems from the difference in electrical conductivity. For n- and p-type doping, the peak of *ZT* value along the *zz* lattice direction is much larger than those, respectively, along the *xx* direction and the *yy* direction. Due to high PFs and low lattice thermal conductivity, at 700 K, maximum *ZT* value along the *zz* lattice direction can reach 1.75 (2.45) in n-type (p-type) doping, which is much larger than that of d-Si (0.06)).[14–16] and Si_{24} (0.6).[48] Overall, our results show that the Si (oP32) is a hopeful candidate for good thermoelectric material.

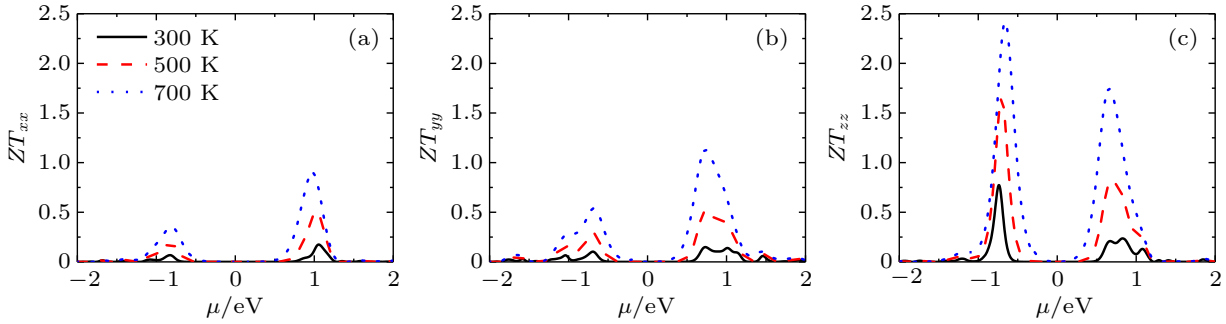


Fig. 6. Plots of thermoelectric figure of merit (*ZT*) *versus* chemical potential along (a) *xx*, (b) *yy*, and (c) *zz* (c) lattice directions of Si (oP32) at different temperatures.

4. Conclusions

In this work, we investigate the electronic structure, phonon, and electron transport properties of recently predicted Si (oP32) by the first-principles calculations and Boltzmann transport theory. The results show that Si (oP32) has intrinsically the low ability to transport phonons . The lattice thermal

conductivity is about 33.77 W/mK at room temperature, which is much lower than that of d-Si. This is mainly due to the low group velocity and phonon relaxation time, which can be further attributed to the increased phonon–phonon scattering (including scattering phase space and strength). Combining the large power factor, the unexpected high thermoelectric performance can be realized in both p- and n-type Si (oP32) in the high temperature region. The maximum ZT at 700 K under n-type (p-type) doping can reach 1.75 (2.45) along the zz direction. The present work indicates that Si (oP32) is a promising candidate for thermoelectric applications, and it could provide useful guidance for the future building thermoelectric devices in experiment.

References

[1] Böttner H, Chen G and Venkatasubramanian R 2006 *MRS Bull.* **31** 211
[2] Majumdar A 2004 *Science* **303** 777
[3] Sales B C 2002 *Science* **295** 1248
[4] Ouyang Y, Zhang Z, Li D, Chen J and Zhang G 2019 *Annalen der Physik* **531** 1800437
[5] Snyder G J and Toberer E S 2008 *Nat. Mater.* **7** 105
[6] Zhang X and Zhao L D 2015 *J. Mater.* **1** 92
[7] Heremans J P, Jovovic V, Toberer E S, Saramat A, Kurosaki K, Charoenphakdee A, Yamanaka S and Snyder G J 2008 *Science* **321** 554
[8] Li T, Yu J, Nie G, Zhang B P and Sun Q 2020 *Nano Energy* **67** 104283
[9] Zhao L D, Lo S H, Zhang Y, Sun H, Tan G, Uher C, Wolverton C, Dravid V P and Kanatzidis M G 2014 *Nature* **508** 373
[10] Min Hong Z G C, Jin Zou 2018 *Chin. Phys. B* **27** 48403
[11] Li Y N, Wu P, Zhang S P, Chen S, Yan D, Yang J G, Wang L and Huai X L 2018 *Chin. Phys. B* **27** 057201
[12] Petter Jelle B, Breivik C and Drolsum Røkenes H 2012 *Sol. Energy Mater. Sol. Cells* **100** 69
[13] Broido D A, Malorny M, Birner G, Mingo N and Stewart D A 2007 *Appl. Phys. Lett.* **91** 231922
[14] Boukai A I, Bunimovich Y, Tahir-Kheli J, Yu J K, Goddard Iii W A and Heath J R 2008 *Nature* **451** 168
[15] Hochbaum A I, Chen R, Delgado R D, Liang W, Garnett E C, Najarian M, Majumdar A and Yang P 2008 *Nature* **451** 163
[16] Bux S K, Blair R G, Gogna P K, Lee H, Chen G, Dresselhaus M S, Kaner R B and Fleurial J P 2009 *Adv. Func. Mater.* **19** 2445
[17] Wang Q, Xu B, Sun J, Liu H, Zhao Z, Yu D, Fan C and He J 2014 *J. Am. Chem. Soc.* **136** 9826
[18] Kim D Y, Stefanoski S, Kurakevych O O and Strobel T A 2015 *Nat. Mater.* **14** 169
[19] Mujica A, Pickard C J and Needs R J 2015 *Phys. Rev. B* **91** 214104
[20] Beekman M, Wei K and Nolas G S 2016 *Appl. Phys. Rev.* **3** 040804
[21] He C, Zhang C, Li J, Peng X, Meng L, Tang C and Zhong J 2016 *Phys. Chem. Chem. Phys.* **18** 9682
[22] Cai X H, Yang Q, Pang Y and Wang M 2020 *Comput. Mater. Sci.* **173** 109441
[23] Oreshonkov A S, Roginskii E M and Atuchin V V 2020 *J. Phys. Chem. Solids* **137** 109219
[24] Tang Z, Litvinchuk A P, Gooch M and Guloy A M 2018 *J . Am. Chem. Soc.* **140** 6785
[25] Blochl P E 1994 *Phys. Rev. B* **50** 17953
[26] Kresse G and Joubert D 1999 *Phys. Rev. B* **59** 1758
[27] Hafner J 2008 *J. Comput. Chem.* **29** 2044
[28] Perdew J P, Burke K and Ernzerhof M 1996 *Phys. Rev. Lett.* **77** 3865
[29] Tran F and Blaha P 2009 *Phys. Rev. Lett.* **102** 226401
[30] Ouyang T, Zhang P, Xiao H, Tang C, Li J, He C and Zhong J 2017 *J. Phys. D: Appl. Phys.* **50** 425501
[31] Zhang P, Ouyang T, Tang C, He C, Li J, Zhang C, Hu M and Zhong J 2018 *Model. Simul. Mater. Sci. Eng.* **26** 085006
[32] Li W, Carrete J, A. Katcho N and Mingo N 2014 *Comput. Phys. Commun.* **185** 1747
[33] Togo A and Tanaka I 2015 *Scr. Mater.* **108** 1
[34] Madsen G K H and Singh D J 2006 *Comput. Phys. Commun.* **175** 67
[35] Bardeen J and Shockley W 1950 *Phys. Rev.* **80** 72
[36] Parrish K D, Jain A, Larkin J M, Saidi W A and McGaughey A J H 2014 *Phys. Rev. B* **90** 235201
[37] Li W, Mingo N, Lindsay L, Broido D A, Stewart D A and Katcho N A 2012 *Phys. Rev. B* **85** 195436
[38] Peng B, Zhang H, Shao H, Lu H, Zhang D W and Zhu H 2016 *Nano Energy* **30** 225
[39] Zhang P, Ouyang T, Tang C, He C, Li J, Zhang C and Zhong J 2020 *Physica E* **118** 113870
[40] Kaasbjerg K, Thygesen K S and Jacobsen K W 2012 *Phys. Rev. B* **85** 115317
[41] Kaasbjerg K, Thygesen K S and Jauho A P 2013 *Phys. Rev. B* **87** 235312
[42] Fan D D, Liu H J, Cheng L, Jiang P H, Shi J and Tang X F 2014 *Appl. Phys. Lett.* **105** 133113
[43] Sun P P, Bai L, Kripalani D R and Zhou K 2019 *NPJ Comput. Mater.* **5** 9
[44] Zhu X L, Hou C H, Zhang P, Liu P F, Xie G and Wang B T 2020 *J. Phys. Chem. C* **124** 1812
[45] Krali E and Durrani Z A K 2013 *Appl. Phys. Lett.* **102** 143102
[46] Jonson M and Mahan G D 1980 *Phys. Rev. B* **21** 4223
[47] Venkatasubramanian R, Siivola E, Colpitts T and O'Quinn B 2001 *Nature* **413** 597
[48] Chae K, Kang S H, Choi S M, Kim D Y and Son Y W 2018 *Nano Lett.* **18** 4748